Hindawi
Shock and Vibration
Volume 2018, Article ID 3262869, 12 pages
https://doi.org/10.1155/2018/3262869

Research Article

A Correction Method of Estimating the Pointing Error for Reflector Antenna

Jie Zhang[1,2] **Jin Huang**[1] **Wei Liang**[1] **Youran Zhang**[1] **Qian Xu**[2] **Letian Yi**[2] **and Congsi Wang**[1]

[1]*Key Laboratory of Electronic Equipment Structure Design, Ministry of Education, Xidian University, Xi'an 710071, China*
[2]*Xinjiang Astronomical Observatory, Chinese Academy, Xinjiang 830011, China*

Correspondence should be addressed to Jin Huang; jhuang@mail.xidian.edu.cn and Congsi Wang; congsiwang@163.com

Received 15 December 2017; Accepted 22 April 2018; Published 30 May 2018

Academic Editor: Francesco Franco

Copyright © 2018 Jie Zhang et al. This is an open access article distributed under the Creative Commons Attribution License, which permits unrestricted use, distribution, and reproduction in any medium, provided the original work is properly cited.

The pointing error caused by the structural deformation of large reflector antennas has become the most challenging problem of antenna servo control. Especially with the increase of the antenna diameter and the working frequency, environmental loads not only make the structure deformation more obvious, but also make the pointing accuracy influenced by deformation more sensitive. In order to solve this problem, accurately estimating the pointing error caused by the structural deformation is the key. Based on the dynamic model of antenna structure and the analyzing model of pointing error, using the displacement information of sampling points on reflector, this paper proposes a correction method to achieve the purpose of accurately estimating the pointing error caused by the structural deformation. Using a 7.3-m Ka band antenna, the results show that the antenna maximum pointing error in theoretical model calculation is 0.0041° at 10m/s wind speed condition; however, the corrected pointing error would be about 0.0054° with considering the modeling error. After compensating the controller, the pointing error could be reduced to only 0.0008° and the performance of antenna pointing was improved.

1. Introduction

The pointing accuracy is one of the most important technical performance indicators of radio telescope which is the main instrument to receive and transmit electromagnetic waves. Qitai 110m radio telescope (QTT), which will be built in Xinjiang, China, has pointing accuracy required to reach 0.0004°. However, due to the environmental load, the pointing error would be different as follows. It is about 0.011° caused by the deformation from the gravity distribution under different conditions. It is about 0.004° caused by the deformation from temperature gradient. And, it is up to 0.024° caused by the deformation from random wind disturbance [1]. These are far beyond its pointing accuracy requirements. Therefore, the accurate estimation of the pointing errors caused by the environmental load is the basis for guaranteeing pointing accuracy of the large reflector antenna.

The study of pointing errors caused by structural deformation under different conditions such as temperature and gravity distribution is relatively mature, because the change of the loads is slow. The laser measurement techniques were used to obtain the root mean square error (RMSE) of the antenna reflector deformation at different pitch angles and estimate the effect of gravity on the deformation of the structure [2]. By using photogrammetric technology, the antenna reflecting surface deformation of 22m antenna at different pitch angles was obtained, and its impact on the electrical performance of antenna pointing was analyzed [3]. For the deformation of the reflecting surface, a structural optimization of large reflector antennas was proposed, which could reduce the effect of the deformation caused by gravity on the pointing accuracy [4]. Based on the load analysis of the finite element model, the reflector deformation information was obtained. And making use of the adjustment of subreflector position, the effective compensation was realized to reduce the antenna pointing error [5]. The subreflector array adjustment was used to achieve the match of the subreflector shape and to compensate for the loss of electrical

performance, which was caused by the main surface deformation from the slow changes such as gravity and temperature [6]. With considering the effect of temperature on the structural deformation, the optimal structure of reflector back frame was obtained by use of topology optimization, which could realize the effective inhibition to structural deformation caused by temperature gradient [7, 8]. An electromechanical coupling analysis method of electromagnetic performance was proposed for the 40m antenna structural deformation in the solar radiation [9]. The result shows that the electromagnetic performance parameters mainly depend on the reflecting surface deformation distribution not the root mean square error of the reflecting surface deformation.

Because of slow change and high repeatability of temperature and gravity effects, it is possible to set up the error table offline whether using finite element software analysis or actual sensors measurement. Thereby, it could be overcome by look-up table method in the process of antenna servo control. However, as a random transient load which is more difficult to analyze and inhibit, the wind disturbance has also received widespread attention.

The servo error data produced by the wind disturbance of specific antenna location was collected, and the equivalent torque coefficient of wind disturbance at equivalent disturbance torque was derived, which played a guiding role in the wind disturbance simulation in other antenna design [10]. According to the characteristics of wind disturbance on the antenna, the influence of wind disturbance on the antenna pointing was introduced into the simulation analysis, which could be equivalent to three kinds of disturbance forms which are the wind disturbance acting on the reflector surface of the antenna, the torque disturbance acting on the motor shaft of the antenna, and the speed disturbance acting on the velocity loop input [11]. All of them have achieved good simulation results. The finite element software was used to analyze the structural deformation of the 40m antenna at different wind speeds, and the multi-field coupled model was proposed to analyze the pointing error caused by the structural deformation [12]. An antenna dynamic model was introduced to analyze the influence of the deformation of different structures on the pointing error. The result revealed that the pointing error caused by the flexible deformation of the antenna cannot be ignored [13]. Using the beam waveguide system, a fast active compensation structure was designed, and through the optimized selection of the amplification factor, it is possible to quickly compensate for the pointing error caused by wind disturbance [14].

In recent years, although the pointing error of the structural deformation caused by wind disturbance has gradually received attention. The analysis method could be either obtaining structural deformation by the finite element software simulation to estimate the pointing error, however, it cannot be directly applied to the controller implementation, or establishing pointing error analysis model based on the modal superposition method and the approximate optical method, but this method depends on the accuracy of the model which is hard to guarantee for the load model error from the complicate wind pressure distribution on the antenna reflecting surface caused by the turbulent

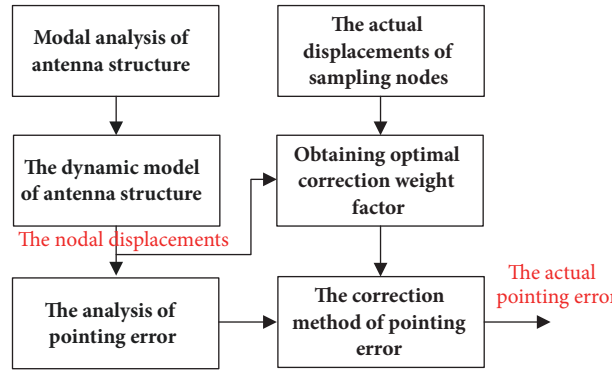

Figure 1: The flow chart of the correction method.

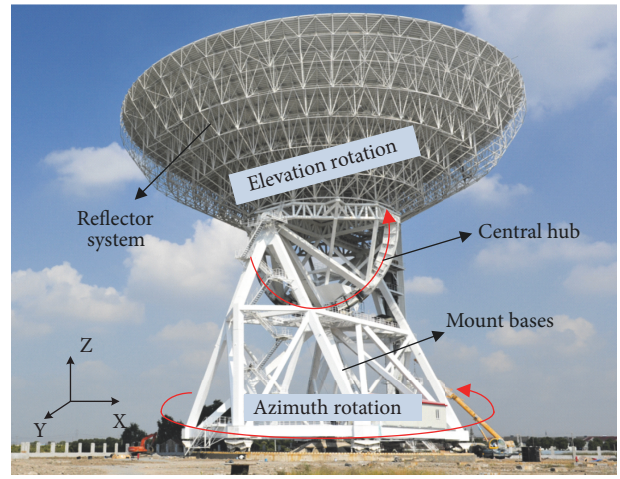

Figure 2: The structure of dual reflector antenna.

characteristics of the wind field and the dynamic model error. It often brings a burden to the design of the controller.

This paper presents a correction method of estimating the pointing error caused by flexible deformation of antennas. The flow chart of this algorithm is shown as Figure 1, based on the establishment of dynamic model of antenna structure and the analysis of pointing error; it constructs pointing error correction method according to the actual displacements of sampling nodes of reflection surface. By modifying the optimal correction weight factor, it eventually achieves the purpose of accurate estimation of the pointing error.

2. The Dynamic Model of Antenna Structure

To analyze the pointing error caused by the environmental load, the first step is to obtain the deformation of the antenna structure under the environmental load. As shown in Figure 2, taking a large dual reflector antenna as an example, the structure consists of the mount base, the central hub, and the reflector system. Any deformation of the parts of the antenna structure will lead to the deflection of the antenna pointing. The deformation of the mount base and the central hub can eventually be reflected in the deflection of the reflector system. As long as we obtain the final position of

each node of the reflector system, the antenna error caused by the deformation of the structure can be synthetically estimated.

The dynamic model of antenna structure under generalized coordinates can be expressed as follows [15]:

$$\mathbf{M}\ddot{\mathbf{q}} + \mathbf{D}\dot{\mathbf{q}} + \mathbf{K}\mathbf{q} = \mathbf{B}_0\mathbf{u} \tag{1}$$

$$\mathbf{y} = \mathbf{C}_\mathbf{o}\mathbf{q} \tag{2}$$

where the diagonal matrices, $\mathbf{M}$, $\mathbf{K}$, and $\mathbf{D}$, are the mass matrix, stiffness matrix, and damping matrix, respectively. The environment load inputs of the flexible model is u. The output vector, $\mathbf{y}$, is obtained by the nodal displacement vector, $\mathbf{q}$. $\mathbf{B}_0$ is the input matrix and $\mathbf{C}_0$ is the output matrix.

To express the structure in modal coordinates, the modal displacement is introduced, which satisfies the following equations:

$$\mathbf{q} = \Phi\mathbf{q}_\mathbf{m}. \tag{3}$$

Φ is the modal shape matrix consisting of the jth node displacement of the ith mode, ϕ_{ij}.

$$\Phi = \begin{bmatrix} \phi_{11} & \phi_{21} & \cdots & \phi_{\mathbf{n}1} \\ \phi_{12} & \phi_{22} & \cdots & \phi_{\mathbf{n}2} \\ \cdots & \cdots & \cdots & \cdots \\ \phi_{1\mathbf{k}} & \phi_{2\mathbf{k}} & \cdots & \phi_{\mathbf{n}\mathbf{k}} \\ \cdots & \cdots & \cdots & \cdots \\ \phi_{1\mathbf{n_d}} & \phi_{2\mathbf{n_d}} & \cdots & \phi_{\mathbf{n}\mathbf{n_d}} \end{bmatrix}. \tag{4}$$

Introducing (3) into (1) and (2), and multiplying by $\Phi^\mathbf{T}$, the dynamic equation based on modal coordinate could be obtained:

$$\mathbf{M}_\mathbf{m}\ddot{\mathbf{q}}_\mathbf{m} + \mathbf{D}_\mathbf{m}\dot{\mathbf{q}}_\mathbf{m} + \mathbf{K}_\mathbf{m}\mathbf{q}_\mathbf{m} = \Phi^\mathbf{T}\mathbf{B}_0\mathbf{u} \tag{5}$$

$$\mathbf{y} = \mathbf{C}_\mathbf{o}\Phi\mathbf{q}_\mathbf{m}. \tag{6}$$

The mass matrix, stiffness matrix, and damping matrix were transformed into modal mass matrix, $\mathbf{M}_\mathbf{m}$, modal stiffness matrix, $\mathbf{K}_\mathbf{m}$, and modal damping matrix $\mathbf{D}_\mathbf{m}$, respectively:

$$\mathbf{M}_\mathbf{m} = \Phi^\mathbf{T}\mathbf{M}\Phi \tag{7}$$

$$\mathbf{K}_\mathbf{m} = \Phi^\mathbf{T}\mathbf{K}\Phi \tag{8}$$

$$\mathbf{D}_\mathbf{m} = \Phi^\mathbf{T}\mathbf{D}\Phi. \tag{9}$$

Meanwhile, the input matrix and output matrix are transformed into modal input matrix, $\mathbf{B}_\mathbf{m}$, and modal output matrix $\mathbf{C}_\mathbf{m}$.

$$\Phi^\mathbf{T}\mathbf{B}_0 = \mathbf{B}_\mathbf{m} = \begin{bmatrix} b_{m1} \\ b_{m2} \\ \cdots \\ b_{mi} \end{bmatrix} \tag{10}$$

$$\mathbf{C}_\mathbf{o}\Phi = \mathbf{C}_\mathbf{m} = \begin{bmatrix} c_{m1} & c_{m2} & \cdots & c_{mi} \end{bmatrix}. \tag{11}$$

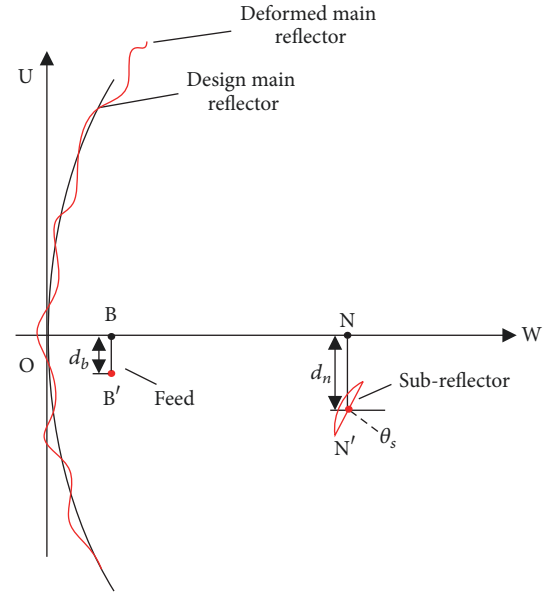

Figure 3: The factors influencing the performances of antenna pointing.

The modal mass matrix and modal stiffness matrix satisfy the following equation, where Ω is the natural frequency matrix and ω_i is the frequency of ith order.

$$\Omega^2 = \mathbf{M}_\mathbf{m}{}^{-1}\mathbf{K}_\mathbf{m} \tag{12}$$

$$\Omega = \begin{bmatrix} \omega_1 & 0 & \cdots & 0 \\ 0 & \omega_2 & \cdots & 0 \\ \cdots & \cdots & \cdots & \cdots \\ 0 & 0 & \cdots & \omega_\mathbf{n} \end{bmatrix}. \tag{13}$$

The modal damping ratio matrix, $\mathbf{Z}$, could be expressed as (14), and the transfer function of the ith mode is obtained from (15).

$$\mathbf{Z} = \begin{bmatrix} \xi_1 & 0 & \cdots & 0 \\ 0 & \xi_2 & \cdots & 0 \\ \cdots & \cdots & \cdots & \cdots \\ 0 & 0 & \cdots & \xi_\mathbf{n} \end{bmatrix} = 0.5\mathbf{M}_\mathbf{m}{}^{-1}\mathbf{D}_\mathbf{m}\Omega^{-1} \tag{14}$$

$$g_{li}(\omega) = \frac{c_{mi}b_{mi}}{\omega_i{}^2 - \omega^2 + 2j\xi_i\omega_i\omega}. \tag{15}$$

3. The Analysis of Pointing Error Caused by Structure Deformation

To dual reflector antenna, the factors influencing the performances of antenna pointing include the deformation of the main reflector, the lateral displacement (perpendicular to the focal axis) of the feed, the lateral displacement, and the rotation of the subreflector, as shown in Figure 3.

When analyzing the influence of the deformed main reflector on pointing error, the best fitting paraboloid should be obtained based on the displacement of each node of the reflector. There are six key parameters to confirm the best fitting paraboloid. They are the displacement of the vertex of the fitted parabolic reflector, d_u, d_v, d_w, the rotation angles of the focal axis of the fitted parabolic reflector, ϕ_u, ϕ_v, and the variation in the focal length, d_f.

The relationship among these parameters and the displacement of each node could be expressed as follows [16]:

$$A_n\beta = H_n \tag{16}$$

where

$$A_n = \begin{bmatrix} \sum_{s=1}^{n}\frac{u_s^2}{2f} & \sum_{s=1}^{n}\frac{u_s v_s}{2f} & -\sum_{s=1}^{n}u_s & -\sum_{s=1}^{n}u_s v_s & \sum_{s=1}^{n}u_s^2 & \sum_{s=1}^{n}\frac{u_s w_s}{f} \\ \sum_{s=1}^{n}\frac{u_s v_s}{2f} & \sum_{s=1}^{n}\frac{v_s^2}{2f} & -\sum_{s=1}^{n}v_s & -\sum_{s=1}^{n}v_s^2 & \sum_{s=1}^{n}u_s v_s & \sum_{s=1}^{n}\frac{v_s w_s}{f} \\ \sum_{s=1}^{n}\frac{u_s w_s}{2f} & \sum_{s=1}^{n}\frac{v_s w_s}{2f} & -\sum_{s=1}^{n}w_s & -\sum_{s=1}^{n}v_s w_s & \sum_{s=1}^{n}u_s w_s & \sum_{s=1}^{n}\frac{w_s^2}{f} \\ \sum_{s=1}^{n}\frac{u_s}{2f} & \sum_{s=1}^{n}\frac{v_s}{2f} & -n & -\sum_{s=1}^{n}v_s & \sum_{s=1}^{n}u_s & \sum_{s=1}^{n}\frac{w_s}{f} \end{bmatrix} \tag{17}$$

$$H_n = \left[\sum_{s=1}^{n}\left(w_s - w_s'\right)u_s \quad \sum_{s=1}^{n}\left(w_s - w_s'\right)v_s \quad \sum_{s=1}^{n}\left(w_s - w_s'\right)w_s \quad \sum_{s=1}^{n}\left(w_s - w_s'\right)\right]^T \tag{18}$$

$$\beta = \left[d_u \;\; d_v \;\; d_w \;\; \phi_u \;\; \phi_v \;\; d_f\right]^T \tag{19}$$

where u_s, v_s, w_s is the design coordinate of sth node, w_s' is the coordinate after deformation along the direction of focal axis, and f is the length of the focal axis.

As shown in Figure 4, after obtaining the best fitting paraboloid, the pointing error in azimuth direction caused by the lateral displacement of the vertex, d_u, the rotation angle of the focal axis ϕ_v, the lateral displacement of the feed d_b, the lateral displacement of the subreflector d_n, and the rotation angle of the subreflector θ_s could be obtained using the following equations.

The distance between B′ and the focal axis of the subreflector is d_{s1}, which leads to a lateral displacement d_{s2}:

$$d_{s1} = \cos\theta_s\left|d_b + d_n + \tan\theta_s L_1\right| \tag{20}$$

$$d_{s2} = \frac{d_{s1}L_3}{L_1} \tag{21}$$

where L_1 is the distance between points B and N, and L_3 is the distance between points N′ and F.

K_w is the beam deviation factor, which is related to the ratio of the paraboloid focal distance to its open diameter and aperture-field distribution. By omitting the vertex displacement of the paraboloid along the W axis, the actual pointing error caused by structural deformation can be expressed as θ_n:

$$d_o = \frac{\left|\tan\phi_v\left(L_1 + L_3\cos\theta_s - d_{s2}\sin\theta_s\right) - \left(d_n + L_3\sin\theta_s + d_{s2}\cos\theta_s\right) + \tan\phi_v L_2 - d_u\right|}{\sqrt{1 + \left(\tan\phi_v\right)^2}} \tag{22}$$

$$\theta_d = \phi_v - \frac{d_o K_w}{f} \tag{23}$$

4. Correction Method of Estimating the Pointing Error

During the estimation of the pointing error θ_n, it is hard to accurately obtain the input of the environment loads because of the complexity of wind field. Meanwhile, taking the modeling error of dynamic model into account, it usually leads to some unavoidable estimation error of the pointing error. As a result, θ_n needs to be corrected.

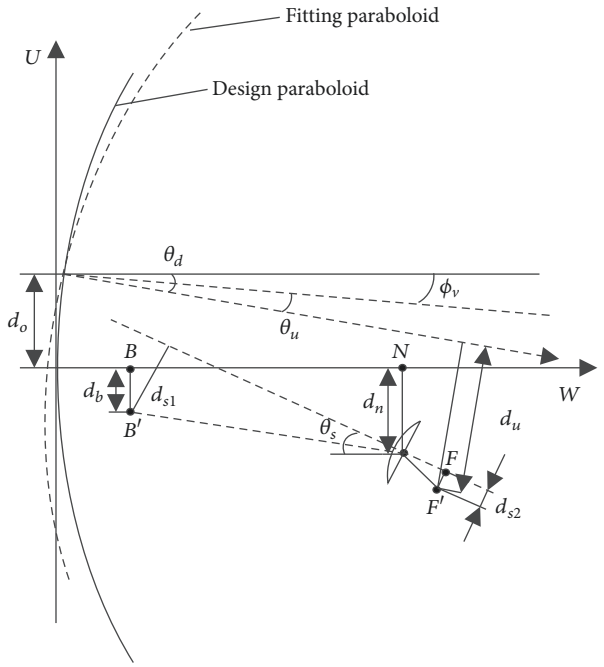

Figure 4: The pointing error caused by reflector deformation.

From (6), the node displacement could be obtained by the superposition of displacement of each mode, so the displacement of lth node could be expressed as follows:

$$s_l = \sum_{i=1}^{n} C_o \Phi q_i = \sum_{i=1}^{n} y_{li} \tag{24}$$

where y_{li} is the displacement of the ith mode. So the pointing error could also be expressed as follows:

$$\theta_d = \sum_{i=1}^{n} \theta_i \tag{25}$$

where θ_i is the pointing error of ith mode. Assuming the actual pointing error, $\theta_d{}'$, is obtained by

$$\theta_d{}' = \sum_{i=1}^{n} (1 + \alpha_i)\, \theta_i \tag{26}$$

where α_i is correction weight factor of each mode. The actual displacement, $s_l{}'$, of lth node could be obtained.

$$s_l{}' = \sum_{i=1}^{n} \left(1 + \frac{\alpha_i}{\gamma_i}\right) y_{li} \tag{27}$$

where γ_i is the gain from node displacement to pointing error of ith mode; it could be defined as follows:

$$\gamma_i = \frac{\theta_i}{y_{li}} = \frac{\theta_i}{u} \times \frac{u}{y_{li}} = \left\| g_{zi} \right\|_2 \times \frac{1}{\left\| g_{li} \right\|_2} \tag{28}$$

g_{zi} is the transfer function from environment loads to pointing error, and g_{li} is the transfer function from environment loads to node displacement as shown in (15). $\| \cdot \|_2$ denotes the H2 norm of the transfer function.

To simplify the pointing error expression, omitting the effect of the high-order term as (29), g_{zi} could be obtained from (30).

$$d_{s2}\theta_s \approx 0 \tag{29}$$

$$\begin{aligned} g_{zi} = {} & \left(\mathbf{A}^{-1}{}_{5,1} \sum_{l=1}^{n} g_{li} u_s + \mathbf{A}^{-1}{}_{5,2} \sum_{l=1}^{n} g_{li} v_s \right. \\ & \left. + \mathbf{A}^{-1}{}_{5,3} \sum_{l=1}^{n} g_{li} w_s + \mathbf{A}^{-1}{}_{5,4} \sum_{l=1}^{n} g_{li} \right) \\ & - \left| \left(\mathbf{A}^{-1}{}_{5,1} \sum_{l=1}^{n} g_{li} u_s + \mathbf{A}^{-1}{}_{5,2} \sum_{l=1}^{n} g_{li} v_s \right. \right. \\ & \left. + \mathbf{A}^{-1}{}_{5,3} \sum_{l=1}^{n} g_{li} w_s + \mathbf{A}^{-1}{}_{5,4} \sum_{l=1}^{n} g_{li} \right) (L_1 + L_3) - \left(g_{iB} \right. \\ & \left. \left. + L_3 g_{i\theta} + \frac{L_3 \left| g_{iN} + g_{iB} + L_1 g_{i\theta} \right|}{L_1} \right) \right. \\ & + L_2 \left(\mathbf{A}^{-1}{}_{5,1} \sum_{l=1}^{n} g_{li} u_s + \mathbf{A}^{-1}{}_{5,2} \sum_{l=1}^{n} g_{li} v_s \right. \\ & \left. + \mathbf{A}^{-1}{}_{5,3} \sum_{l=1}^{n} g_{li} w_s + \mathbf{A}^{-1}{}_{5,4} \sum_{l=1}^{n} g_{li} \right) - \left(\mathbf{A}^{-1}{}_{1,1} \sum_{l=1}^{n} g_{li} u_s \right. \\ & \left. \left. + \mathbf{A}^{-1}{}_{1,2} \sum_{l=1}^{n} g_{li} v_s + \mathbf{A}^{-1}{}_{1,3} \sum_{l=1}^{n} g_{li} w_s + \mathbf{A}^{-1}{}_{1,4} \sum_{l=1}^{n} g_{li} \right) \right| \\ & \cdot K_w / f \end{aligned} \tag{30}$$

where g_{iB} is the transfer function from the environment loads to the displacement of the feed of the ith mode, g_{iN} is the transfer function from the environment loads to the displacement of the subreflector of the ith mode, and $g_{i\theta}$ is the transfer function from the environment loads to the rotation angel of the subreflector of ith mode.

$$\begin{aligned} & \left[\mathbf{A}^{-1}{}_{51} \;\; \mathbf{A}^{-1}{}_{52} \;\; \mathbf{A}^{-1}{}_{53} \;\; \mathbf{A}^{-1}{}_{54} \right] \\ & = \left[0 \;\; 0 \;\; 0 \;\; 0 \;\; 1 \;\; 0 \right] \mathbf{A_n}^{-1} \end{aligned} \tag{31}$$

$$\begin{aligned} & \left[\mathbf{A}^{-1}{}_{11} \;\; \mathbf{A}^{-1}{}_{12} \;\; \mathbf{A}^{-1}{}_{13} \;\; \mathbf{A}^{-1}{}_{14} \right] \\ & = \left[1 \;\; 0 \;\; 0 \;\; 0 \;\; 0 \;\; 0 \right] \mathbf{A_n}^{-1} \end{aligned} \tag{32}$$

The H_2 norm of each transfer function could be derived, respectively:

$$\|g_{li}\|_2 = \frac{\|c_{mi}\|_2 \|b_{mi}\|_2}{2\sqrt{\xi_i \omega_i}} \tag{33}$$

$$\begin{aligned}\|g_{zi}\|_2 \approx{}& \frac{|b_{mi}|}{2\sqrt{\xi_i w_i}} \left(1 + \frac{(L_1 + L_3) K_w}{f} + \frac{K_w}{f}\right) \\ &\cdot \sqrt{\left(\mathbf{A}^{-1}{}_{5,1}\right)^2 \sum_{s=1}^{n} \left(c_{mqis} u_s\right)^2 + \left(\mathbf{A}^{-1}{}_{5,2}\right)^2 \sum_{s=1}^{n} \left(c_{mqis} v_s\right)^2 + \left(\mathbf{A}^{-1}{}_{5,3}\right)^2 \sum_{s=1}^{n} \left(c_{mqis} w_s\right)^2 + \left(\mathbf{A}^{-1}{}_{5,4}\right)^2 \sum_{s=1}^{n} \left(c_{mqis}\right)^2} + \frac{K_w |b_{mi}|}{2f\sqrt{\xi_i w_i}} \\ &\cdot \sqrt{c_{mqiN}{}^2 + L_3{}^2 c_{mqi\theta}{}^2} + \frac{K_w L_3 |b_{mi}|}{2 f L_1 \sqrt{\xi_i w_i}} \sqrt{c_{mqiB}{}^2 + c_{mqiN}{}^2 + L_1{}^2 c_{mqi\theta}{}^2} + \frac{K_w |b_{mi}|}{2f\sqrt{\xi_i w_i}} \\ &\cdot \sqrt{\left(\mathbf{A}^{-1}{}_{1,1}\right)^2 \sum_{s=1}^{n} \left(c_{mqis} u_s\right)^2 + \left(\mathbf{A}^{-1}{}_{1,2}\right)^2 \sum_{s=1}^{n} \left(c_{mqis} v_s\right)^2 + \left(\mathbf{A}^{-1}{}_{1,3}\right)^2 \sum_{s=1}^{n} \left(c_{mqis} w_s\right)^2 + \left(\mathbf{A}^{-1}{}_{1,4}\right)^2 \sum_{s=1}^{n} \left(c_{mqis}\right)^2}\end{aligned} \tag{34}$$

where c_{mqiB} is the ith mode of node B which is the central point of the feed, c_{mqiN} is the ith mode of the modal output matrix of node N which is the central point of the subreflector, and $c_{mqi\theta}$ is the ith mode of the modal output matrix which is for deriving the rotation angle of the subreflector.

When the node displacements, $s_1, s_2, ..., s_l$, of the limited sampling points are obtained, to obtain the optimal correction weight factor, the sum δ_s given in the following should have its smallest value. And the actual pointing error, $\theta_d{}'$, could be derived after the correction weight factor determined.

$$\delta_s = \sqrt{\frac{\sum_{i=1}^{l} \left(s_i - s_i{}'\right)^2}{l}} \tag{35}$$

5. Model Application

Taking the antenna with a diameter of 7.3 meters as an example, the antenna and its finite element model are shown in Figure 5. The finite element model is used to derive modal information (modal matrices) of the structure, which lays a foundation for the dynamic model. What is more, some tests are used to prove that the finite element model of the antenna was compliant with a real antenna, and some analytical results indicate that the proposed model is effective. Next, it is explained in detail.

5.1. Experimental Testing. In order to verify the accuracy of the finite element model, a frequency test experiment and a load deformation experiment are made to the antenna.

A load deformation experiment is applied by the 100Kg impulse in lateral loading and vertical loading, respectively. As shown in Figure 6, red arrows represent load action direction. Deformation testing equipment is the laser tracker (API). An example of field testing is shown in Figure 7. Numeral 1 represents the API laser tester. Numeral 2 represents the target location. Numeral 3 represents 100Kg load. Three sets of testing were done at elevation angles of 30°, 50°, and 70°, respectively. Comparing the ANSYS finite element simulation results and API test results, the static maximum deformation and the pointing error in the deformation process are shown in Table 1. The relative error represents the ratio of the absolute pointing error and the test results of pointing error.

Take the dynamic process into account, taking elevation angle of 70°, for example, API test results and simulation results are compared as shown in Figure 8.

It can be seen from the comparison of the results that static load deformation error is less than 20% and dynamic response characteristics are basically consistent.

Frequency test experiments were performed in two directions by loading impulse loads (to generate oscillations of the antenna structure in the two directions). The oscillation directions corresponding to orientation and elevation were adopted, and accelerometer sensors were placed on the two points with the largest amplitudes. Then, by using the modal analyzer, the natural frequencies in the two directions were acquired by analyzing the data collected by the accelerometer sensors and comparing the results with those of the ANSYS model with the same oscillation modal (with the same oscillation). Table 2 shows a comparison of the test results and simulation results.

From the results of frequency test experiment and load deformation experiment, it is considered that the finite element analysis results basically meet the accuracy requirement. The finite element model can be used as a basis for dynamic modeling and reference for real-testing structural deformation.

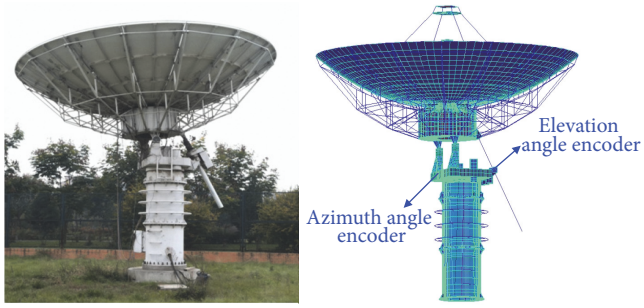

Figure 5: The real and finite element model of 7.3m antenna.

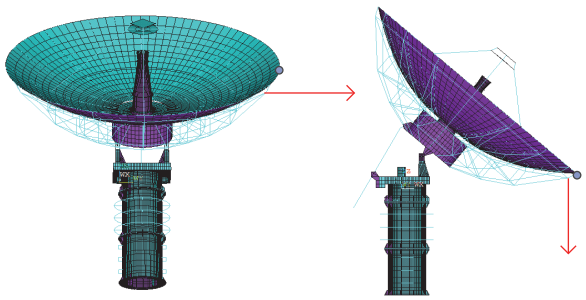

Figure 6: The position and direction of the applied load.

5.2. Numerical Calculation. For pointing error simulation analysis, taking a random disturbance as an example, the average wind speed is 10m / s according to the spectrum characteristics of wind disturbance. The equivalent wind force acting laterally on the 7.3m antenna reflector is shown in Figure 9.

The maximum pointing error is about 0.0041°, which caused by the structural deformation under the wind disturbance, by applying the pointing error analysis model described in this article, see Figure 10.

Because the wind disturbance modeling error is not considered in the above-mentioned pointing error estimation, the correction method described in the article will be used to correct the pointing error.

Suppose the reflector system uniformly distributes 15 deformation sampling points; see Figure 11.

When the wind disturbance modeling error is not introduced, the node deformation is calculated from the dynamic model described in this paper; see Figure 12. Due to the symmetry of the reflector system and the loading action, it only selects number 1, 2, 5, 9, 10, and 14 node displacements for comparison; x1, x2, x5, x9, x10, and x14 are the corresponding node deformation, respectively.

The finite element software analysis results replace the actual deformation information in pointing error correction. In the process of the finite element analysis, the load modeling error is introduced, by the transient analysis of the ANSYS software, the deformation of the nodes (s1, s2, s5, s9, s10, and s14) is shown in Figure 13.

Figure 7: An example of field testing.

5.3. Analytical Results. The deformation information of these nodes is regarded as the measured deformation information. The correction method proposed in this paper is used to correct the pointing error shown in Figure 10. Comparing the correction result of pointing error before and after, it can be seen that the maximum value of the pointing error is 0.0041° which is obtained by relying solely on the pointing error analysis model as shown in Figure 14. After considering the wind disturbance model error, the corrected pointing error is 0.0054°.

According to the correction of estimating the pointing error caused by the structural deformation, a controller is designed as shown in Figure 15 (PID controller is the most common techniques in engineering projects).

Under a wind with the speed of 10 m/s, Figure 16 shows the pointing performances of the antenna servo system with PID controller. Before the compensation of the pointing error caused by wind pressure, the maximum pointing error would be up to 0.0054°. But the maximum pointing error is only about 0.0008° by introducing $\theta_a{}'$ into controller of the position loop. Therefore, it is necessary to propose a method to estimate the pointing error caused by wind accurately.

6. Conclusion

The influence of the large reflector antenna flexible deformation on the pointing accuracy has become more and more significant. The traditional pointing error estimation method either depends on finite element software analysis and thus cannot be directly applied to pointing control, or depends on the modeling accuracy of the load model and the pointing error analysis model and thus cannot guarantee the accuracy of the error estimation. Against these problems, this paper proposes a correction method of pointing error caused by structural deformation based on optimization of correction weight factor of each order of pointing error. Through the experiment and simulation of the 7.3m antenna, it shows that the method can effectively correct the pointing error estimation by using the measured deformation, consequently

Table 1: The comparison of static maximum deformation and the pointing error.

Loading direction	EL angle	Simulation results of deformation (mm)	Simulation results of pointing error (")	Test results of deformation (mm)	Test results of pointing error (")	Relative error (%)
Lateral direction	70	0.80	2.88	0.68	2.41	19.50%
	50	0.66	1.80	0.55	1.52	18.42%
	30	0.41	1.13	0.50	1.36	16.91%
Vertical direction	70	1.30	4.32	1.23	4.11	5.11%
	50	1.45	5.04	1.44	4.89	3.07%
	30	1.63	6.12	1.52	6.30	4.44%

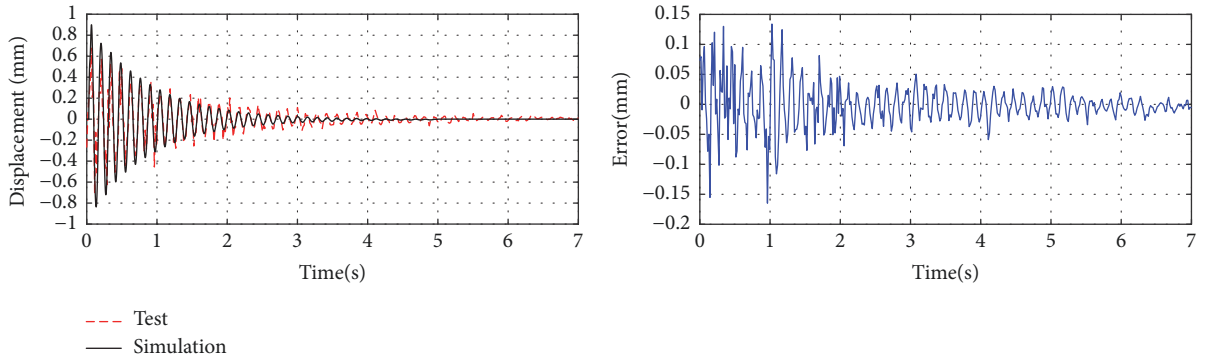

(a) The dynamic oscillatory in time domain

(b) The error between test and simulation

Figure 8: The comparison of the dynamic oscillatory of the sampling point.

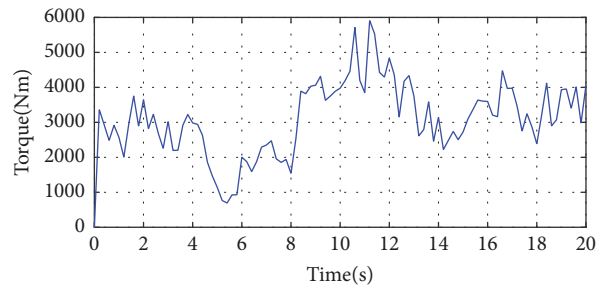

Figure 9: The equivalent wind force acting laterally on reflector.

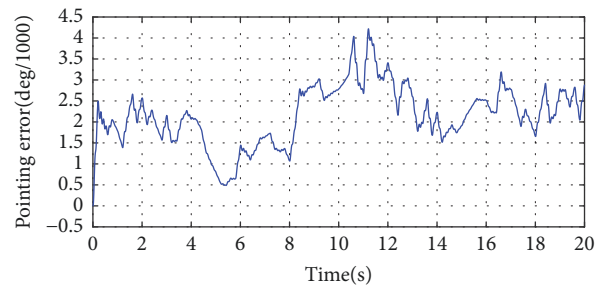

Figure 10: The pointing error caused by deformation of the reflector.

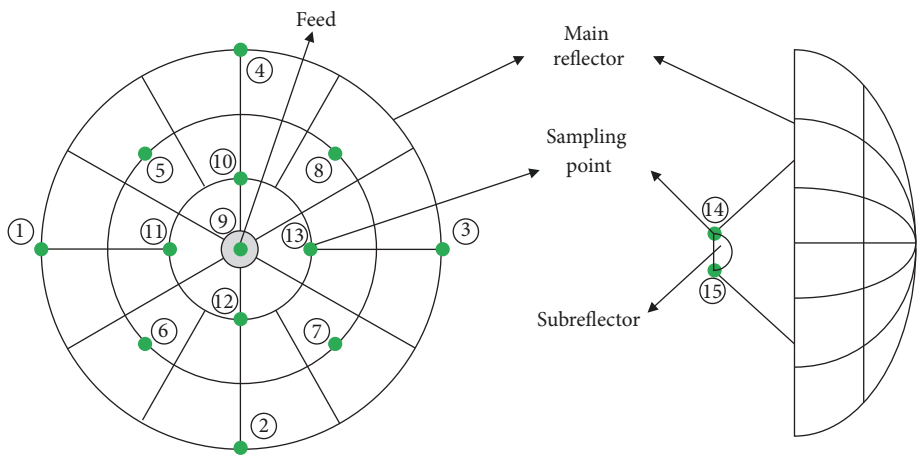

Figure 11: The distribution of sampling points on the reflector.

Table 2: Natural frequency measurement tests.

Test content	Load (kg)	Test result (Hz)	Simulation result (Hz)	Relative error (%)
Rotation mode in EL	100	6.84	7.625	11.48
Rotation mode in EL	50	6.84	7.625	11.48
Rotation mode in AZ	100	27.34	26.893	1.63
Rotation mode in AZ	50	27.34	26.893	1.63

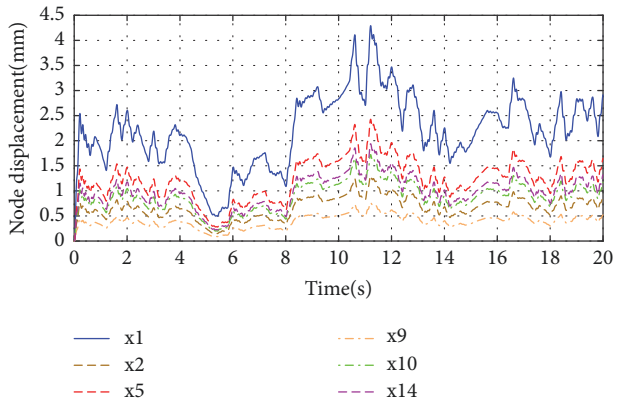

Figure 12: The nodal displacement obtained from dynamic model.

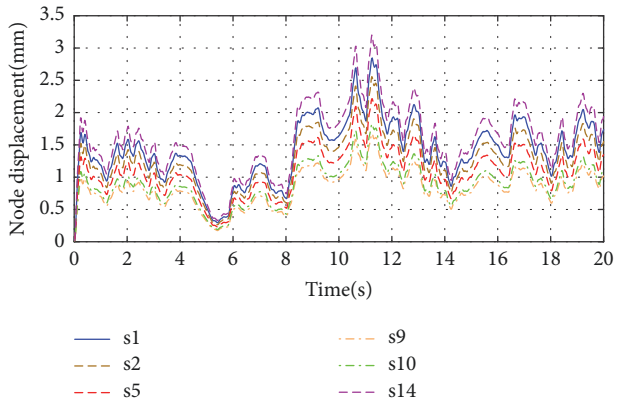

Figure 13: The nodal displacement with considering the load modeling error.

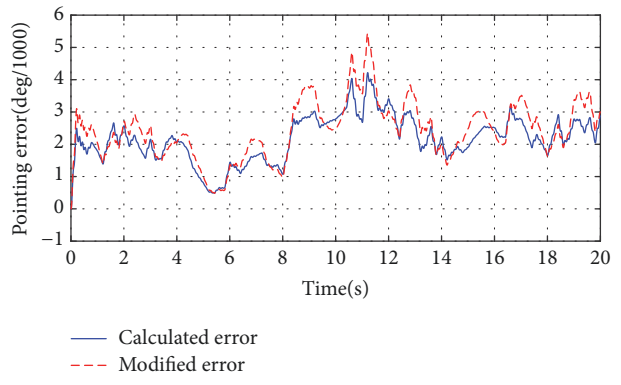

Figure 14: The comparison of pointing error before and after the correction.

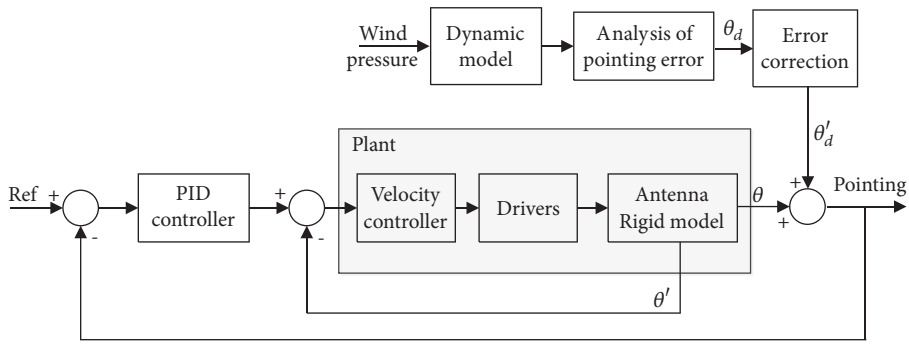

Figure 15: Antenna servo system.

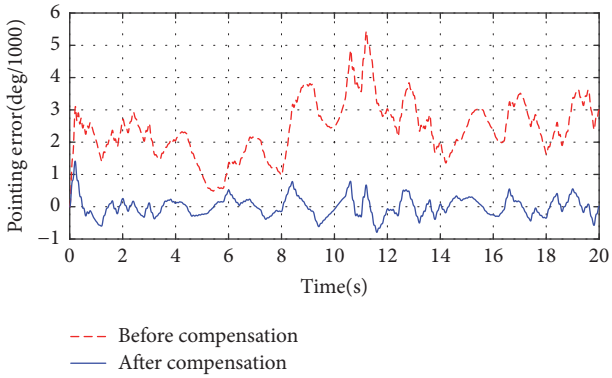

Figure 16: The pointing performance after compensation.

to improve the accuracy of the pointing error after compensation with PID controller.

Conflicts of Interest

The authors declare that they have no conflicts of interest.

Acknowledgments

This work was supported by the National 973 Program under Grant no. 2015CB857100, the National Natural Science Foundation of China under Grant nos. 51705387, 51575419, and 51490660, the National 111 Project under Grant no. B14042, the China Postdoctoral Science Foundation under Grant no. 2017M613078, the Fundamental Research Funds for the Central Universities under Grant no. JBX170414, and the CAS "Light of West China" Program under Grant nos. 2017-XBQNXZ-B-024 and 2017-XBQNXZ-B-023.

References

[1] J. Zhang, J. Huang, R. Song, and L. Qiu, "Analysis of reflector vibration-induced pointing errors for large antennas subject to wind disturbance," *IEEE Antennas and Propagation Magazine*, vol. 57, no. 6, pp. 46–61, 2015.

[2] M. Brenner, M. J. Britcliffe, and W. A. Imbriale, "Gravity deformation measurements of 70 m reflector surfaces," *IEEE Antennas and Propagation Magazine*, vol. 44, no. 6, pp. 187–192, 2001.

[3] R. Subrahmanyan, "Photogrammetric measurement of the gravity deformation in a Cassegrain antenna," *IEEE Transactions on Antennas and Propagation*, vol. 53, no. 8, pp. 2590–2596, 2005.

[4] C. S. Wang, B. Y. Duan, and Y. Y. Qiu, "On distorted surface analysis and multidisciplinary structural optimization of large reflector antennas," *Structural and Multidisciplinary Optimization*, vol. 33, no. 6, pp. 519–528, 2007.

[5] W. Wang, C. Wang, B. Duan, and G. Leng, "Compensation for gravity deformation via subreflector motion of 65 m shaped Cassegrain antenna," *Microwaves Antennas and Propagation letter*, vol. 8, no. 3, pp. 158–164, 2013.

[6] S. Xu, Y. Rahmat-Samii, and W. A. Imbriale, "Subreflectarrays for reflector surface distortion compensation," *IEEE Transactions on Antennas and Propagation*, vol. 57, no. 2, pp. 364–372, 2009.

[7] N. Hu, H. Bao, B. Duan, G. Yang, and Y. Zong, "Topology optimization of reflector antennas based on integrated thermal-structural-electromagnetic analysis," *Structural and Multidisciplinary Optimization*, pp. 1–8, 2016.

[8] C. S. Wang, B. Y. Duan, F. S. Zhang, and M. B. Zhu, "Coupled structural-electromagnetic-thermal modelling and analysis of active phased array antennas," *IET Microwaves, Antennas & Propagation*, vol. 4, no. 2, pp. 247–257, 2010.

[9] P. Li, B. Y. Duan, W. Wang, and F. Zheng, "Electromechanical coupling analysis of ground reflector antennas under solar radiation," *IEEE Antennas and Propagation Magazine*, vol. 54, no. 5, pp. 40–57, 2012.

[10] W. Gawronski, J. A. Mellstrom, and B. Bienkiewicz, "Antenna mean wind torques: A comparison of field and wind-tunnel data," *IEEE Antennas and Propagation Magazine*, vol. 47, no. 5, pp. 55–59, 2005.

[11] W. Gawronski, "Modeling wind-gust disturbances for the analysis of antenna pointing accuracy," *IEEE Antennas and Propagation Magazine*, vol. 46, no. 1, pp. 50–58, 2004.

[12] B. Y. Duan and C. S. Wang, "Reflector antenna distortion analysis using MEFCM," *IEEE Transactions on Antennas and Propagation*, vol. 57, no. 10, pp. 3409–3413, 2009.

[13] J. Zhang, J. Huang, J. Zhou, C. Wang, and Y. Zhu, "A compensator for large antennas based on pointing error estimation under a wind load," *IEEE Transactions on Control Systems Technology*, vol. 5, no. 25, pp. 1912–1920, 2017.

[14] J. Zhang, J. Huang, S. Wang, and C. Wang, "An active pointing compensator for large beam waveguide antenna under wind disturbance," *IEEE/ASME Transactions on Mechatronics*, vol. 21, no. 2, pp. 860–871, 2016.

[15] W. Gawronski, "Analytical models," in *Modeling and Control of Antennas and Telescopes*, pp. 13–50, Springer, New York, NY, USA, 2004.

[16] C. S. Wang, B. Y. Duan, and Y. Y. Qiu, "Precise algorithm for surface errors of reflector antennas and analysis of its electrical performance," *Chinese Journal of Radio Science*, vol. 21, pp. 23–28, 2006.

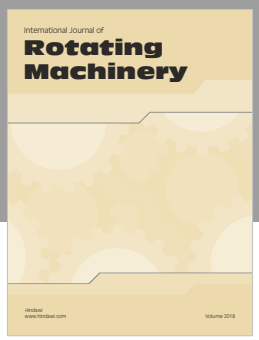

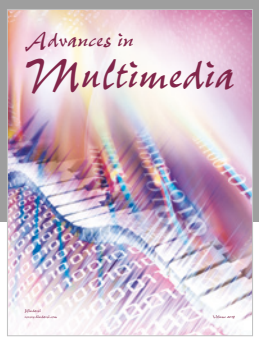

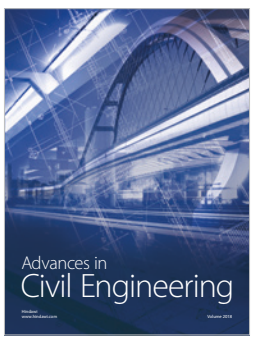

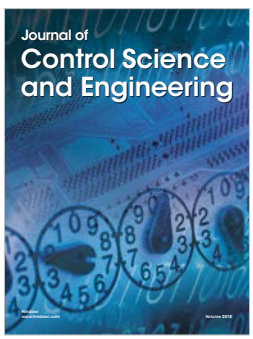

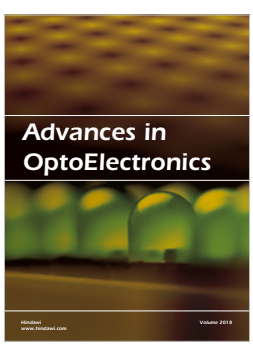

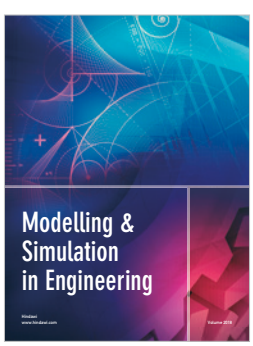

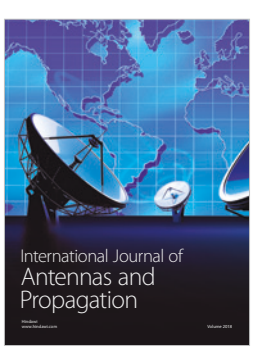

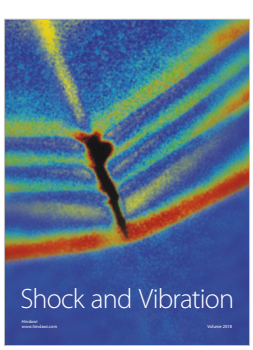

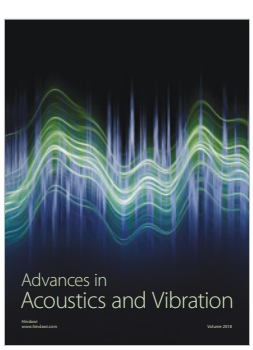

Hindawi

Submit your manuscripts at
www.hindawi.com